



Sub-decibel silicon grating couplers based on L-shaped waveguides and engineered subwavelength metamaterials

DANIEL BENEDIKOVIC,^{1,*} CARLOS ALONSO-RAMOS,¹ SYLVAIN GUERBER,^{1,2}
XAVIER LE ROUX,¹ PAVEL CHEBEN,³ CÉCILIA DUPRÉ,⁴ BERTRAND
SZELAG,⁴ DAVID FOWLER,⁴ ÉRIC CASSAN,¹ DELPHINE MARRIS-MORINI,¹
CHARLES BAUDOT,² FRÉDÉRIC BOEUF,² AND LAURENT VIVIEN,¹

¹Centre de Nanosciences et de Nanotechnologies, CNRS, Université Paris-Sud, Université Paris-Saclay, 91120 Palaiseau, France

²Technology R&D, STMicroelectronics SAS, 850 Rue Jean Monnet, 38920 Crolles, France

³National Research Council Canada, Ottawa, ON K1A 0R6, Canada

⁴University Grenoble Alpes and CEA, LETI, Minatèc Campus, F-38054 Grenoble, France

*daniel.benedikovic@c2n.upsaclay.fr

Abstract: The availability of low-loss optical interfaces to couple light between standard optical fibers and high-index-contrast silicon waveguides is essential for the development of chip-integrated nanophotonics. Input and output couplers based on diffraction gratings are attractive coupling solutions. Advanced grating coupler designs, with Bragg or metal mirror underneath, low- and high-index overlays, and multi-level or multi-layer layouts, have proven less useful due to customized or complex fabrication, however. In this work, we propose a rather simpler in design of efficient off-chip fiber couplers that provide a simulated efficiency up to 95% (-0.25 dB) at a wavelength of $1.55\text{ }\mu\text{m}$. These grating couplers are formed with an *L*-shaped waveguide profile and synthesized subwavelength grating metamaterials. This concept jointly provides sufficient degrees of freedom to simultaneously control the grating directionality and out-radiated field profile of the grating mode. The proposed chip-to-fiber couplers promote robust sub-decibel coupling of light, yet contain device dimensions ($> 120\text{ nm}$) compatible with standard lithographic technologies presently available in silicon nanophotonic foundries. Fabrication imperfections are also investigated. Dimensional offsets of $\pm 15\text{ nm}$ in shallow-etch depth and $\pm 10\text{ nm}$ in linewidth's and mask misalignments are tolerated for a 1-dB loss penalty. The proposed concept is meant to be universal, which is an essential prerequisite for developing reliable and low-cost optical couplers. We foresee that the work on *L*-shaped grating couplers with sub-decibel coupling efficiencies could also be a valuable direction for silicon chip interfacing in integrated nanophotonics.

© 2019 Optical Society of America under the terms of the [OSA Open Access Publishing Agreement](#)

1. Introduction

Silicon-on-insulator (SOI) has become a prominent material platform that has proved useful for monolithic nanophotonic integration. Using silicon (Si) as a waveguide core enables the realization of compact components with unique prospects in chip complexity, integration density, and manufacturing volumes [1–8].

However, scaling device size towards sub-micrometer dimensions complicates optical chip interfacing, particularly due to the largely disparate mode dimensions of Si waveguides and standard single-mode optical fibers [9–13]. This imposes a serious hurdle for high-speed interconnects, communication links and hubs, as well as quantum information sciences, among others. The presence of efficient input and output optical interfaces drives the development in SOI nanophotonics and also remains a very active area of research [11–13],

where optical couplers based on inverse tapers [14–20] and diffraction gratings [21–57] are routinely adopted solutions.

Edge couplers [14–20], with a high coupling efficiency and low polarization sensitivity are favorable for wideband applications, although they significant require post-fabrication treatment. Wafer dicing, high-quality facet preparation, and high-resolution optical alignment are drawbacks of facet couplers, making them less-suited for on-wafer testing. Surface grating couplers [21–57], on the other hand, are narrowband and polarization selective devices. They afford a number of distinctive advantages, which strongly facilitate both integration [21,22] and packaging [23,24]. This includes flexible placement on the chip surface and rapid circuits testing using automated wafer-scale accessories. Moreover, the out-of-plane couplers are typically more forgiving to alignment variation in fiber attachments.

Extensive research on grating coupler designs has been reported over recent years. Generally, there are two factors that combine together to hamper overall fiber-to-chip coupling: the fiber-grating field profile mismatch and the light leakage towards bottom Si substrate [11–13]. The former is overcome by grating coupler apodization, while the latter typically require more complex design interventions. To prevent the light leakage towards Si substrate, the thin-film interference at the interface between the buried oxide (BOX) and the Si substrate can be exploited. In particular, substantially improved coupling efficiency has been achieved by forming bottom mirrors embedded at the chip backside via Bragg [21,23,34–36] or metal mirrors [37–40], respectively. However, local BOX thinning, backside wafer processing, or flip-chip bonding introduce additional complexity in fabrication and increase the production cost. Alternatively, the efficiency can also be improved by breaking the vertical device symmetry [41–57]. The out-of-plane asymmetry favors improved coupling in a desired direction (typically towards optical fiber situated above the chip), while minimizing the light radiation into the Si substrate. Different approaches have been devised, including low- and high-index overlays [41–44], multi-layer, and multi-level grating architectures [45–50]. Although low-loss fiber-to-chip couplers have been reported, such designs typically require either customized SOI substrates or intended process steps, which however, differ considerably from recent standards in open-access platform offerings through foundry sharing initiatives [7,8].

Most recently, we have proposed and experimentally demonstrated efficient grating couplers that exploit the unique blasing effect by using only dual-etch fabrication process [51,52]. Here, the radiation performance is controlled through a set of asymmetric scatterers that yield constructive (destructive) interference in the upwards (downwards) direction. Surface grating couplers with interleaved [51–53] and *L*-shaped [54–57] waveguide geometries have been reported, both showing a broader potential for efficient fiber-to-chip coupling. Moreover, blazed dual-etch grating couplers are easy to design and can also be exploited in different waveguide platforms [56,57]. Despite advances achieved recently, as far as we are aware, surface grating couplers with a robust sub-decibel performance and device layouts compatible with industrial-scale manufacturing have yet to be developed. Here, we propose off-chip fiber couplers that meet such challenges and could present a valuable route for Si chip interfacing with zero changes to the existing manufacturing flow.

2. Grating coupler optimization

Schematic views of the proposed chip-to-fiber grating coupler are shown in Fig. 1. The coupler design is implemented on SOI platform with 300-nm Si (h_w), 720-nm BOX, and a silicon dioxide (SiO_2) as a surrounding medium. The refractive index of Si and SiO_2 is 3.476 and 1.444, respectively. The grating coupler is based on *L*-shaped geometry with full ($h_w = 300$ nm) and shallow ($h_e = 150$ nm) etch trenches. The diffraction structure is defined via the grating period (A) with deep- and partial-etch trenches (with lengths l_d and l_s), and a non-etched Si slab (with length l_n). Fiber-to-chip grating couplers are designed for transverse electric (TE) polarization and operation at 1.55 μm wavelength. For device design and entire

optimization, we used tools based on Finite Difference Time Domain (FDTD) [58] and Fourier-based Eigenmode Expansion (F-EEM) [59] methods. Since grating couplers are wider than thicker ($W_g = 15 \mu\text{m} \gg h_w = 300 \text{ nm}$, in particular), they can be effectively modeled in two-dimensions (2-D). Yet results provide very good agreement with rigorous three-dimensional (3-D) calculations [52,54].

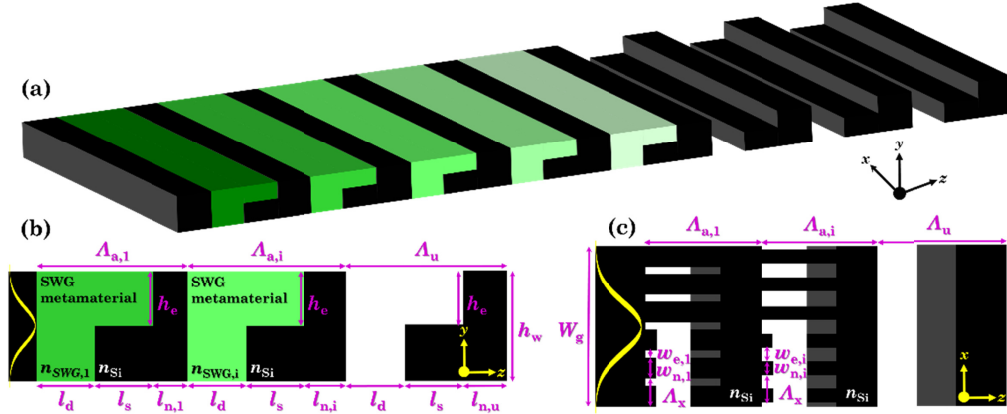


Fig. 1. (a) Three-dimensional (3-D) and de-coupled two-dimensional (2-D) (b) side and (c) top view schematics of the proposed fiber-to-chip grating coupler with an L-shaped waveguide profile and engineered subwavelength grating (SWG) metamaterials embedded within the etched trenches.

The proposed grating coupler consists of an apodized and a uniform section. As shown in Fig. 1, the apodized region comprises full- and shallow-etch trenches with a synthesized subwavelength grating (SWG) metamaterial, followed by a uniform coupler region (deep and shallow trenches are filled by a superstrate medium). This way, the grating directionality and the grating strength can be controlled simultaneously. The overall grating structure (l_{gc}) used in numerical optimization can be expressed as:

$$l_{gc} = \sum_{i=1}^{NP_a} \Lambda_{a,i} + NP_u \cdot \Lambda_u \quad (1)$$

Here, NP_a and NP_u are numbers of periods within the apodized and the uniform coupler section ($NP = NP_a + NP_u$), respectively. Here, NP is total number of grating periods, which is fixed to 30. $\Lambda_{a,i}$ and Λ_u are local grating periods for apodized and uniform section, respectively, and i is the integer number that corresponds to the apodized period.

The grating directionality, defined as the ratio between the optical power diffracted towards optical fiber and the power radiated into the Si substrate, strongly depends on the lengths of deep-etch (l_d) and shallow-etch (l_s) trenches as well as on a non-etched Si slab (l_n). The grating strength is altered with equivalent metamaterials that vary gradually along the axis of light propagation (here, z -axis) to achieve a field matching between profiles of the diffracted grating mode and the near-Gaussian mode of the standard single-mode optical fiber. The mode field diameter of $10.4 \mu\text{m}$ is assumed, defined at $1/e^2$ intensity drop and a wavelength of $1.55 \mu\text{m}$. Synthesized metamaterials comprising periodic arrangements of Si segments also called sub-wavelength gratings (SWGs), are nanophotonic structures with dimensions on a scale near or below the wavelength of light propagating through it, thereby preventing Bragg resonances and frustrating all diffraction orders, except the zero-th order [60]. These non-resonant metamaterials are implemented perpendicularly to the direction of light propagation (along the x -axis, see Figs. 1(a) and 1(c)). The refractive index of equivalent metamaterials is determined as an intermediate refractive index between that of alternating segments of core (Si) and surrounding (SiO_2) materials. By controlling widths of etched (w_e)

and non-etched (w_n) holes within a SWG period ($\Lambda_x = w_e + w_n$, $\Lambda_x = 450$ nm) of the non-resonant periodic structure, various refractive indexes can be synthesized [26–30]. In this design, the outstanding radiation performance of L-shaped grating coupler is virtually decoupled from the adjustment of the coupling strength. Yet, such a device arrangement provides sufficient degrees of freedom to tailor the amplitude and the phase of radiated fields, thereby controlling the overall coupling performance.

The grating coupler performance (that is coupling loss, η) is calculated as follows:

$$\eta [dB] = 10 \cdot \log_{10} ((1-R) \cdot (D) \cdot (FM)) \quad (2)$$

Here, R is the reflectivity, D is the directionality, and FM is the field matching between the grating field and the optical fiber mode.

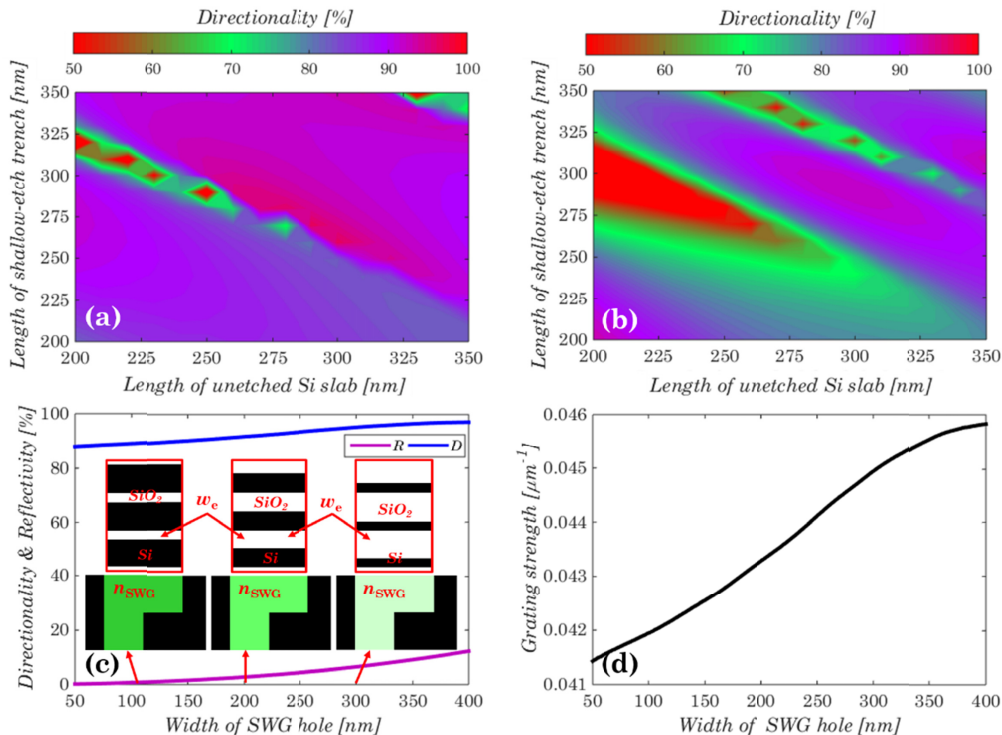


Fig. 2. 2-D mapping of the grating directionality as a function of the unetched Si slabs and the shallow-etch trenches for different lengths of the deep-etch trenches: (a) $l_d = 50$ nm and (b) $l_d = 150$ nm. (c) Grating directionality / grating reflectivity and (d) coupling strength as a function of the width of the etched lateral SWG holes. Inset of (c) synthesis of SWG metamaterials.

Figures 2(a) and 2(b) show the 2-D maps of the directionality for an uniform grating coupler as a function of longitudinal parameters (lengths of the shallow-etch grating trenches (l_s) and the unetched grating teeth (l_u) for two different lengths of the deep-etch grating trenches (l_d) of 50 nm and 150 nm). The calculations suggest that a directionality close to 100% is achieved for a wide range of grating geometries. As a reference, the uniform grating coupler has the following parameters: $l_d = 120$ nm, $l_s = 290$ nm, and $l_u = 300$ nm, $\Lambda_u = 710$ nm, and the total number of grating periods (NP) is 30. Such grating coupler dimensions provide a good trade-off between the grating directionality and minimum feature size requirements, as well as are consistent with our previous work [54]. The nominal radiation angle (Θ) is 17°. The coupling strength is estimated to be $0.047 \mu\text{m}^{-1}$, resulting in an exponentially decaying field profile that yields fiber-grating mode matching efficiency of

76%. The 3-D FDTD calculations predict coupling loss of -2.1 dB at 1.55 μm , with a directionality of 98% and a large return losses in excess of 16% (-8 dB).

Figures 2(c) and 2(d) show the evolution of the grating directionality, the grating reflectivity, and the grating strength as a function of the width of the etched lateral holes (w_e). Throughout the grating coupler optimization, lengths of deep-etch (l_d) and shallow-etch (l_s) trenches are fixed to 120 nm and 290 nm, respectively, while dimensions of unetched Si slabs ($l_{n,i}$) are varied according to the phase-matching condition. In the case of an apodized L -shaped grating coupler with synthesized metamaterials, the following condition holds:

$$l_{n,i} = \frac{k \cdot \lambda}{n_{bf,i} - n_c \cdot \sin(\Theta_i)} - (l_d + l_s) \quad (3)$$

where, k is the grating diffraction order ($k = 1$), λ is the operating wavelength, $n_{bf,i}$ is the effective index of the Bloch-Floquet mode in the grating region, and n_c is the refractive index of the cladding. The local grating period ($A_i = l_d + l_s + l_{n,i}$) is chirped to maintain a linear phase of the radiated grating field and a constant radiation angle ($\Theta = 17^\circ$) along the coupler. Apodization of L -shaped grating couplers using synthesized SWG metamaterials allows to judiciously conform amplitude and phase properties of radiated grating fields, which in turn, enables full control over the grating coupler performance. More specifically, as observed in Fig. 2(c), the directionality of the L -shaped waveguide coupler remains large enough (here, $> 88\%$) for a wide range of lateral SWG geometries, i.e. over a wide span of synthesized SWG metamaterials. Moreover, at the same time, the grating return loss is markedly reduced as a result of the lowered index mismatch at the junction between the input Si waveguide and the grating coupler region. On the other hand, as shown in Fig. 2(d), the coupling strength of the L -shaped grating coupler indicates a steep evolution as the minimum feature size of the etched holes increases, i.e. the refractive index of the synthesized SWG metamaterial decreases, which in turn, increases the grating strength. This allows gradual variation of the coupling strength along the length of the grating coupler.

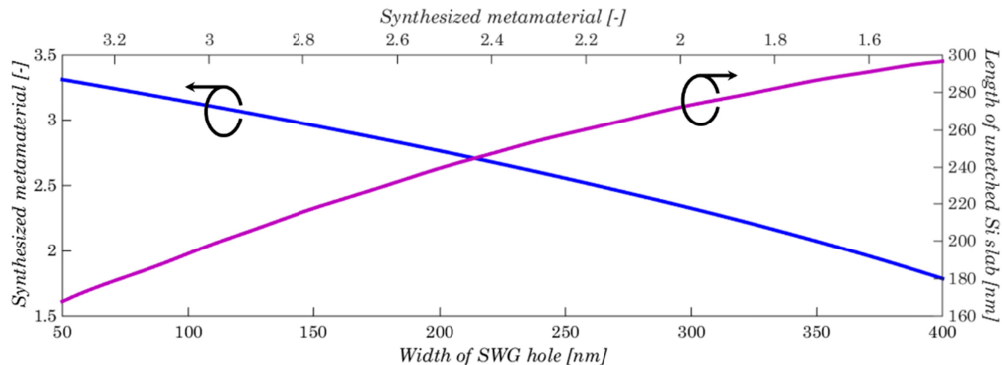


Fig. 3. Relation between the transversal and the longitudinal parameters of the proposed L -shaped grating couplers with index-engineered SWG metamaterials.

Figure 3 shows the relation between the transversal grating dimension (w_e), the synthesized metamaterial index (n_{SWG}), and the longitudinal grating dimension (l_n). This inter-dependent relation between transversal and longitudinal parameters serves as a look-up table to provide the exact dimensions of the grating coupler, which when combined together with Eqs. (1) and (3) are steps used in the grating coupler optimization.

3. Optimization results

L -shaped grating couplers with engineered SWG metamaterials can provide a high coupling efficiency to a standard single-mode optical fibers. Figure 4(a) summarizes the calculated

coupling loss between an integrated Si waveguide coupler and an optical fiber. The 2-D mapping of coupling loss, its peak value, is calculated at a nominal wavelength of $1.55\text{ }\mu\text{m}$ as a function of the number of apodized grating periods (NP_a) and the width of the etched SWG holes (w_e), as the later dimensions are of critical interest in practice.

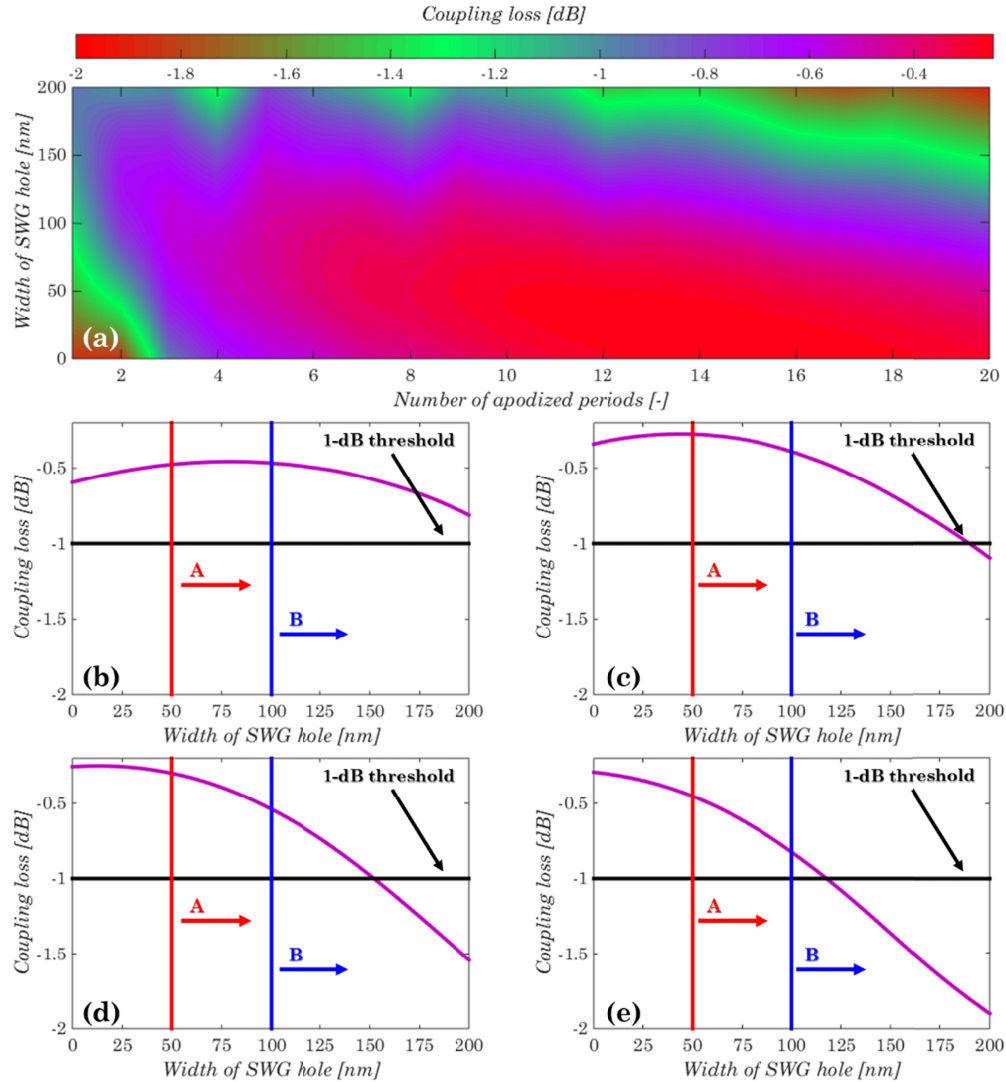


Fig. 4. (a) 2-D mapping of the fiber-to-chip coupling loss as a function of the number of apodized grating periods and the width of the etched SWG hole. Coupling loss versus the width of the etched SWG hole for different number of apodized grating periods: (b) $NP_a = 5$, (c) $NP_a = 10$, (d) $NP_a = 15$, and (e) $NP_a = 20$. In panels (b) to (e), the horizontal line (solid black) represents a 1-dB loss threshold in fiber-to-chip coupling, while two vertical lines (solid red and blue) denote minimum feature size that can be fabricated by using state-of-the-art patterning technologies (immersion {A} and deep-ultraviolet {B} optical lithography's) used in Si nanophotonic foundries.

It is observed that a wide set of grating coupler designs can be chosen, with a coupling loss below 1 dB. For instance, a grating coupler design with only one apodized period already predicts coupling loss of 1 dB for a minimum feature size in excess of 160 nm. As compared to a reference grating coupler design (uniform grating coupler without a synthesized

metamaterial) with coupling loss of -2.1 dB, the grating coupler apodization improves the overall device performance by 1 dB.

Detailed inspection of the fiber-to-chip coupling loss for the proposed *L*-shaped grating couplers is shown in Figs. 4(b) – 4(e). Here, the coupling loss as a function of the width of the etched SWG hole are plotted, with a horizontal line (solid black) for a 1-dB threshold and two vertical lines (solid red and blue, respectively). Two vertical lines correspond to minimum critical dimensions of established lithographic technologies available in nanophotonic foundries. Specifically, minimum feature size of 50 -nm for electron-beam (e-beam) [61] and high-end immersion lithography [8], while lowest dimension of 100 -nm for 193 -nm deep-ultraviolet (deep-UV) optical lithography [54,62], are considered. Indeed, with a continual improvement in lithographic technologies, 193 -nm deep-UV's with sub- 100 -nm resolution, 80 -nm in particular, are also accessible in Si-foundry-compatible nanophotonic platforms [3,21,22].

As shown in Fig. 4(b), an *L*-shaped grating coupler with a 5 apodized periods provides a peak fiber-to-chip coupling at a critical dimension of 80 nm, with a corresponding loss of -0.45 dB. This is also associated with an exceptionally low coupling loss penalty of only ~ 0.35 dB for an ultra-wide range of minimum feature size, spanning from 50 nm up to 200 nm. Furthermore, the increase of the number of apodized grating periods improves the peak coupling loss up to -0.25 dB (95% of coupling efficiency) for a 50 -nm minimum feature size (see Fig. 4(c)). It is also observed that grating coupler designs with a larger number of apodized periods (see Figs. 4(d) and 4(e)) shift the peak coupling loss below the limit of critical dimensions that are considered in this work (< 50 nm). Moreover, for grating coupler designs with a large number of apodized periods, the range of critical dimensions, for which the robust sub-decibel coupling of light can be obtained is continually reduced. The drop in fiber-chip coupling loss is more pronounced for a larger number of apodized periods and larger features of the lateral SWG holes. As the grating directionality remains exceptionally high, in a range of 95% to 99% in particular, the reduction in coupling loss is attributed to the increased coupling strength of the waveguide grating coupler, which in turn, yields a non-optimal mode matching between the radiated grating field and the Gaussian-like fiber mode. Nevertheless, according to our calculations, a robust 1-dB threshold is reached at critical device features of about 190 nm, 150 nm, and 120 nm for optimized grating coupler designs comprising 10 , 15 , and 20 apodized periods, respectively. The presented grating coupler designs are well-suited to maintain sub-decibel coupling losses for substantially relaxed critical dimensions (> 120 nm). The fact that *L*-shaped grating couplers can be made with such feature sizes is also a promising prospect for ever-improving fabrication process fidelity. These resolutions correspond to lithographic technologies used by established fabrication nodes in CMOS pilot lines and foundries [8].

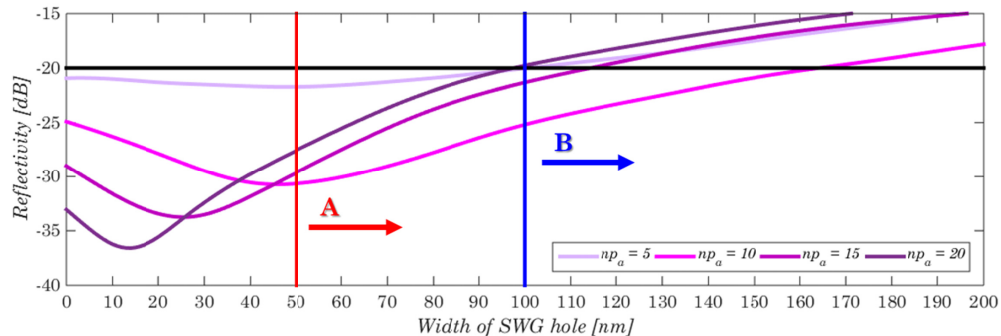


Fig. 5. Grating reflectivity as a function of the width of the etched SWG hole for different number of apodized grating periods. Two vertical lines (solid red and blue) denote minimum feature criteria for immersion {A} and deep-ultraviolet {B} lithographies.

The grating reflectivity as a function of the width of the etched lateral hole is shown in Fig. 5. Calculations are carried out for different coupler designs with various number of apodized periods ($NP_a = 5, 10, 15$, and 20). The reflectivity of couplers is typically below -20 dB for minimum feature size of 100 nm, near a design wavelength of 1.55 μm . Indeed, it is observed that the grating reflectivity strongly depends on the critical dimensions. As the minimum feature size decreases, the reflectivity is reduced, and vice versa. Small device features yield high refractive index of the synthesized SWG metamaterials in deep- and shallow-etch grating trenches, which in turn, improves the mismatch between effective indexes of the injection waveguide mode and Bloch-Floquet mode of the apodized grating coupler. The grating couplers with very low reflectivity (down to -37 dB) require critical dimensions that are below the considered fabrication limit (< 50 nm).

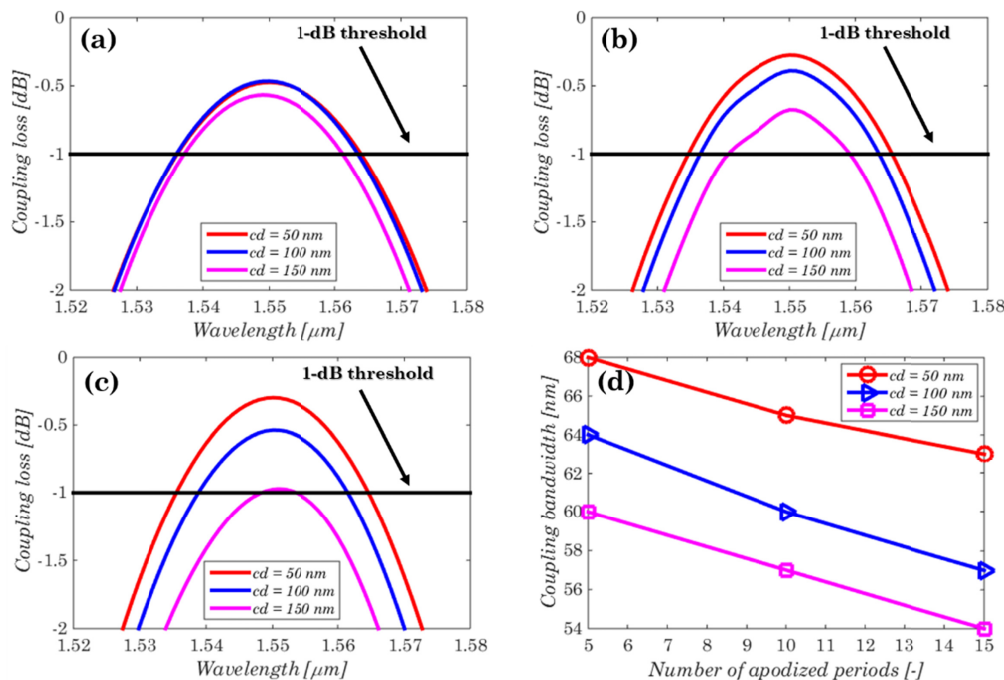


Fig. 6. Coupling loss as a function of the wavelength for different critical dimensions and various number of apodized grating periods: (a) $NP_a = 5$, (b) $NP_a = 10$, and (c) $NP_a = 15$. (d) Summarized 3-dB coupling bandwidth of the apodized *L*-shaped fiber-to-chip grating couplers as a function of the number of apodized periods and various minimum feature sizes.

Figure 6 shows the calculated coupling losses of apodized *L*-shaped couplers as a function of the wavelength. The calculations of the wavelength-dependent coupling loss are performed for different grating coupler designs, with a variable number of apodized periods ($NP_a = 5, 10$, and 15) and various criteria on minimum feature size of 50 nm, 100 nm, and 150 nm, respectively. We can see that all grating coupler designs can provide the desired sub-decibel coupling loss. As expected, wavelength-dependent loss increases with the minimum feature size of the lateral SWG holes.

The coupling bandwidth of apodized *L*-shaped grating couplers is wide enough to fully cover wavelengths in the *C*-band communication window. More specifically, the 1-dB and the 3-dB coupling bandwidths are in a range from 29 nm to 40 nm and 54 nm to 68 nm, respectively. Figure 6(d) summarizes 3-dB coupling bandwidth of respective grating coupler designs. The coupling bandwidth is reduced for grating couplers with a larger number of apodized periods' and for designs with enlarged minimum feature sizes. Nevertheless, the coupling bandwidths of apodized *L*-shaped waveguide couplers compare favorably with

previously reported results for conventional grating coupler designs. The bandwidth of *L*-shaped grating couplers can be further enhanced by coupling light to and from an optical fiber of reduced mode field diameter [47,48,63].

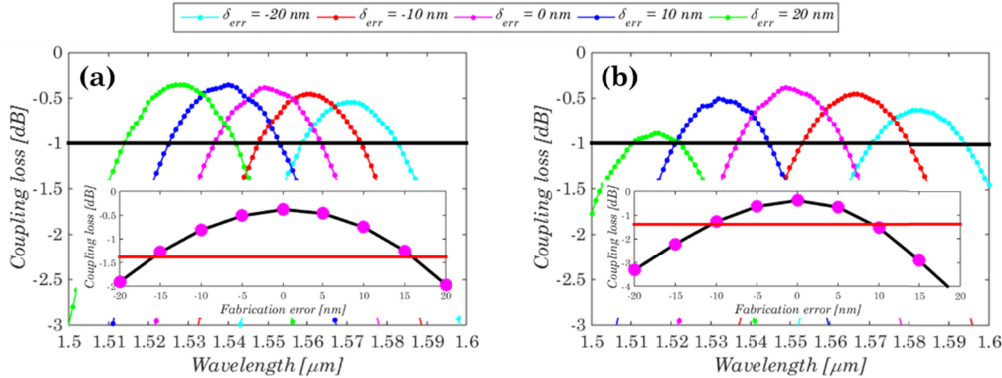


Fig. 7. Tolerance analysis: Coupling loss as a function of a wavelength for grating coupler designs. (a) Etch depth variation and (b) in-plane dimensional variation. Insets: Coupling loss as a function of fabrication errors at a design wavelength of 1.55 μm .

We also evaluate the tolerance of the proposed apodized *L*-shaped grating couplers to fabrication imperfections. Figure 7 shows the fiber-to-chip coupling loss as a function of the wavelength for grating coupler designs taking into the account fabrication errors. Tolerance analysis is performed for a grating coupler design with 10 apodized periods and reference minimum feature size of 100 nm. Fabrication errors, denoted as δ_{err} , in a range of ± 20 nm are considered. The fabrication errors' analysis is de-coupled into the vertical and in-plane device dimensions. The former includes variations in etch depth, whereas the in-plane imperfections encompass changes in lengths of deep-etch (l_d), shallow-etch (l_s) trenches and unetched Si teeth (l_n), in widths of the etched lateral holes (w_e), as well as the mask misalignment (m) between the full and partial etches. For the in-plane device imperfections, the dimensional offsets of ± 20 nm in both transversal and longitudinal directions are assumed for the grating coupler design, thus varying the device lateral features accordingly to the length variations in order to perform a credible tolerance study. The grating structural parameters in the presence of fabrication errors are defined as follows:

$$\begin{aligned} h_e &= h_{e,0} + \delta_{\text{err}} \{h_e\} \\ l_d &= l_{d,0} + \delta_{\text{err}} \{l_d\} \\ l_s &= l_{s,0} + \delta_{\text{err}} \{l_s\} \\ l_n &= l_{n,0} - \delta_{\text{err}} \{l_n\} - \delta_{\text{err}} \{m\} \\ w_e &= w_{e,0} - \delta_{\text{err}} \{w_e\} \end{aligned} \quad (4)$$

where $h_{e,0}$; $l_{d,0}$; $l_{s,0}$; $l_{n,0}$; and $w_{e,0}$ are nominal grating coupler dimensions.

As can be observed in Fig. 7, the proposed *L*-shaped grating couplers are more tolerant to variations in etching depth than to variations in in-plane device dimensions. Specifically, etch level variations of ± 20 nm yield a coupling loss penalty of only ~ 0.16 dB, with notable red and blue spectral shifts. For operation at a central wavelength of 1.55 μm , calculations predict that errors in etch depth of ± 15 nm yields a 1-dB penalty. Conversely, the *L*-shaped fiber couplers are more sensitive to in-plane perturbations, i.e. to the variations in lengths of etched trenches and unetched teeth, in widths of etched SWG holes as well as to the mask misalignment, as shown in Fig. 7(b). For a ± 20 nm variation, the coupling loss drops to 0.91

dB and it is accompanied by noticeable spectral shift. For a 1-dB coupling penalty, dimensional offsets of ± 10 nm are tolerated, as shown in the inset of Fig. 7(b).

4. Conclusions

We proposed an efficient chip-to-fiber grating couplers to enable a low-loss interconnectivity between integrated SOI nanophotonic circuits and standard single-mode optical fibers. The grating couplers were formed with *L*-shaped waveguide profile and synthesized SWG metamaterials. This device arrangement is favorable for providing enough degrees of freedom to alter the grating directionality and radiated field profile, with overall fiber-chip coupling efficiency approaching 95% (-0.25 dB) at a wavelength of $1.55\text{ }\mu\text{m}$. Moreover, apodized *L*-shaped grating couplers were designed for robust sub-decibel coupling and device layouts compatible with lithographic technologies for mass-scale production (> 120 nm). Tolerance analysis suggested that dimensional offsets up to ± 15 nm can be tolerated, with a 1-dB loss penalty. Overall, our work holds promises to further the development of robust, reliable, and low-cost off-chip fiber couplers within available silicon-foundry-compatible processing nodes. This result may provide a crucial edge in building future optical interfaces in large-volume chip-integrated nanophotonics.

Funding

The European Union's Horizon 2020 research and innovation program (ERC POPSTAR – grating agreement N° 647342), partially founded by Agence Nationale de la Recherche (ANR) MIRSPEC, Nano 2020 under Important Projects of Common European Interest (IPCEI).

References

1. P. Cheben, R. Halir, J. H. Schmid, H. A. Atwater, and D. R. Smith, "Subwavelength integrated photonics," *Nature* **560**(7720), 565–572 (2018).
2. J. Chiles and S. Fathpour, "Silicon photonics beyond silicon-on-insulator," *J. Opt.* **19**(5), 053001 (2017).
3. F. Boeuf, S. Crémer, E. Temporiti, M. Feré, M. Shaw, C. Baudot, N. Vulliet, T. Pinguet, A. Mekis, G. Masini, H. Petiton, P. Le Maitre, M. Traldi, and L. Maggi, "Silicon Photonics R&D and Manufacturing on 300-mm Wafer Platform," *IEEE J. Light. Technol.* **34**(2), 286–295 (2016).
4. R. Halir, A. Ortega-Moñux, D. Benedikovic, G. Z. Mashanovich, J. G. Wangüemert-Pérez, J. H. Schmid, I. Molina-Fernández, and P. Cheben, "Subwavelength-Grating Metamaterial Structures for Silicon Photonic Devices," *Proc. IEEE* **106**(12), 2144–2157 (2018).
5. W. Zhou, Z. Cheng, X. Chen, K. Xu, X. Sun, and H. K. Tsang, "Subwavelength engineering in silicon photonic devices," *IEEE J. Sel. Top. Quantum Electron.* **25**(3), 2900113 (2019).
6. C. Doerr and L. Chen, "Silicon Photonics in Optical Coherent Systems," *Proc. IEEE* **106**(12), 2291–2301 (2018).
7. A. Novack, M. Streshinsky, R. Ding, Y. Liu, A. E.-J. Lim, G.-Q. Lo, T. Baehr-Jones, and M. Hochberg, "Progress in silicon platforms for integrated optics," *Nanophotonics* **3**(4–5), 205–214 (2014).
8. A. Rahim, T. Spuesens, R. Baets, and W. Bogaerts, "Open-Access Silicon Photonics: Current Status and Emerging Initiatives," *Proc. IEEE* **106**(12), 2313–2330 (2018).
9. D. Taillaert, W. Bogaerts, P. Bienstman, T. F. Krauss, P. Van Dale, I. Moerman, S. Verstuyft, D. De Messel, and R. Baets, "An out-of-plane grating coupler for efficient butt-coupling between compact planar waveguides and single-mode fibers," *IEEE J. Quantum Electron.* **38**(7), 949–955 (2002).
10. D. Taillaert, P. Bienstman, and R. Baets, "Compact efficient broadband grating coupler for silicon-on-insulator waveguides," *Opt. Lett.* **29**(23), 2749–2751 (2004).
11. G. Son, S. Han, J. Park, K. Kwon, and K. Yu, "High-efficiency broadband light coupling between optical fibers and photonic integrated circuits," *Nanophotonics* **7**(12), 1845–1864 (2018).
12. D. Vermeulen and C. V. Poulton, "Optical Interfaces for Silicon Photonic Circuits," *Proc. IEEE* **106**(12), 2270–2280 (2018).
13. R. Marchetti, C. Lacava, L. Carroll, K. Gradkowski, and P. Minzioni, "Coupling strategies for silicon photonics integrated chips [Invited]," *Photon. Res.* **7**(2), 201–239 (2019).
14. V. R. Almeida, R. R. Panepucci, and M. Lipson, "Nanotaper for compact mode conversion," *Opt. Lett.* **28**(15), 1302–1304 (2003).
15. P. Cheben, D.-X. Xu, S. Janz, and A. Densmore, "Subwavelength waveguide grating for mode conversion and light coupling in integrated optics," *Opt. Express* **14**(11), 4695–4702 (2006).

16. P. J. Bock, P. Cheben, J. H. Schmid, J. Lapointe, A. Delâge, S. Janz, G. C. Aers, D.-X. Xu, A. Densmore, and T. J. Hall, "Subwavelength grating periodic structures in silicon-on-insulator: a new type of microphotonic waveguide," *Opt. Express* **18**(19), 20251–20262 (2010).
17. T. Barwicz, A. Janta-Polczynski, M. Khater, Y. Thibodeau, R. Leidy, J. Maling, S. Martel, S. Engelmann, J. S. Orcutt, P. Fortier, and W. M. J. Green, "An O-band metamaterial converter interfacing standard optical fibers to silicon nanophotonics waveguides," in Optical Fiber Communication Conference (OFC, 2015), paper Th3F.3.
18. P. Cheben, J. H. Schmid, S. Wang, D.-X. Xu, M. Vachon, S. Janz, J. Lapointe, Y. Painchaud, and M.-J. Picard, "Broadband polarization independent nanophotonic coupler for silicon waveguides with ultra-high efficiency," *Opt. Express* **23**(17), 22553–22563 (2015).
19. M. Papes, P. Cheben, D. Benedikovic, J. H. Schmid, J. Pond, R. Halir, A. Ortega-Moñux, G. Wangüemert-Pérez, W. N. Ye, D.-X. Xu, S. Janz, M. Dado, and V. Vašinek, "Fiber-chip edge coupler with large mode size for silicon photonic wire waveguides," *Opt. Express* **24**(5), 5026–5038 (2016).
20. T. Barwicz, B. Peng, R. Leidy, A. Janta-Polczynski, T. Houghton, M. Hhater, S. Kamlapurkar, S. Engelman, P. Fortier, N. Boyer, and W. M. J. Green, "Integrated Metamaterial Interfaces for Self-Aligned Fiber-to-Chip Coupling in Volume Manufacturing," *IEEE J. Sel. Top. Quantum Electron.* **25**(3), 4700313 (2019).
21. A. Mekis, S. Gloeckner, G. Masini, A. Narasimha, T. Pinguet, S. Sahni, and P. De Dobbelaere, "A grating-coupler-enabled CMOS photonics platform," *IEEE J. Sel. Top. Quantum Electron.* **17**(3), 597–608 (2011).
22. C. Kopp, S. Bernabé, B. B. Bakir, J.-M. Fédéli, R. Orobctchouk, F. Schrank, H. Porte, L. Zimmermann, and T. Tekin, "Silicon photonic circuits: On-CMOS integration, fiber optical coupling, and packaging," *IEEE J. Sel. Top. Quantum Electron.* **17**(3), 498–509 (2011).
23. C. Li, K. S. Chee, J. Tao, H. Zhang, M. Yu, and G. Q. Lo, "Silicon photonics packaging with lateral fiber coupling to apodized grating coupler embedded circuit," *Opt. Express* **22**(20), 24235–24240 (2014).
24. L. Carroll, J.-S. Lee, C. Scarcella, K. Grädowski, M. Duperron, H. Lu, Y. Zhao, C. Eason, P. Morrissey, M. Rensing, S. Collins, H. Y. Hwang, and P. O'Brien, "Photonic Packaging: Transforming Silicon Photonic Integrated Circuits into Photonic Devices," *Appl. Sci. (Basel)* **6**(12), 426 (2016).
25. A. Bozzola, L. Carroll, D. Gerace, I. Cristiani, and L. C. Andreani, "Optimising apodized grating couplers in a pure SOI platform to -0.5 dB coupling efficiency," *Opt. Express* **23**(12), 16289–16304 (2015).
26. R. Halir, P. Cheben, S. Janz, D.-X. Xu, I. Molina-Fernández, and J.-G. Wangüemert-Pérez, "Waveguide grating coupler with subwavelength microstructures," *Opt. Lett.* **34**(9), 1408–1410 (2009).
27. R. Halir, P. Cheben, J. H. Schmid, R. Ma, D. Bedard, S. Janz, D.-X. Xu, A. Densmore, J. Lapointe, and I. Molina-Fernández, "Continuously apodized fiber-to-chip surface grating coupler with refractive index engineered subwavelength structure," *Opt. Lett.* **35**(19), 3243–3245 (2010).
28. X. Chen and H. K. Tsang, "Nanoholes grating couplers for coupling between silicon-on-insulator waveguides and optical fibers," *IEEE Photonics J.* **1**(3), 184–190 (2009).
29. W. Zhou, Z. Cheng, X. Sun, and H. K. Tsang, "Tailorable dual-wavelength-band coupling in a transverse-electric-mode focusing subwavelength grating coupler," *Opt. Lett.* **43**(12), 2985–2988 (2018).
30. Y. Tong, W. Zhou, and H. K. Tsang, "Efficient perfectly vertical grating coupler for multi-core fibers fabricated with 193 nm DUV lithography," *Opt. Lett.* **43**(23), 5709–5712 (2018).
31. D. Gostimirovic and W. N. Ye, "An Open-Source Artificial Neural Network Model for Polarization-Insensitive Silicon-on-Insulator Subwavelength Grating Couplers," *IEEE J. Sel. Top. Quantum Electron.* **25**(3), 8200205 (2019).
32. N. Purwaha, A. Atieh, and W. N. Ye, "Broadband and polarization flexible SOI grating coupler based on subwavelength gratings with low back reflections," *OSA Continuum* **2**(4), 1350–1357 (2019).
33. R. Marchetti, C. Lacava, A. Khokhar, X. Chen, I. Cristiani, D. J. Richardson, G. T. Reed, P. Petropoulos, and P. Minzioni, "High-efficiency grating-couplers: demonstration of a new design strategy," *Sci. Rep.* **7**(1), 16670 (2017).
34. D. Benedikovic, P. Cheben, J. H. Schmid, D.-X. Xu, J. Lapointe, S. Wang, R. Halir, A. Ortega-Moñux, S. Janz, and M. Dado, "High-efficiency single etch step apodized surface grating coupler using subwavelength structure," *Laser Photonics Rev.* **8**(6), L93–L97 (2014).
35. Z. Wang, Y. Tang, L. Wosinski, and S. He, "Experimental demonstration of a high-efficiency polarization splitter based on a one-dimensional grating with a Bragg reflector underneath," *IEEE Photonics Technol. Lett.* **22**(21), 1568–1570 (2010).
36. C. Baudot, D. Dutartre, A. Souhaité, N. Vulliet, A. Jones, M. Ries, A. Mekis, L. Verslegers, P. Sun, Y. Chi, S. Cremer, O. Gourhant, D. Benoit, G. Courgoulet, C. Perrot, L. Broussous, T. Pinguet, J. Simiviant, and F. Boeuf, "Low Cost 300 mm double-SOI substrate for low insertion loss 1D & 2D grating couplers," in Proceedings of IEEE 11th International on Group IV Photonics (GFP) (IEEE, 2014), pp. 137 – 138.
37. Y. Ding, C. Peucheret, H. Ou, and K. Yvind, "Fully etched apodized grating coupler on the SOI platform with -0.58 dB coupling efficiency," *Opt. Lett.* **39**(18), 5348–5350 (2014).
38. W. S. Zaoui, A. Kunze, W. Vogel, M. Berroth, J. Butschke, F. Letzkus, and J. Burghartz, "Bridging the gap between optical fibers and silicon photonic integrated circuits," *Opt. Express* **22**(2), 1277–1286 (2014).
39. L. Carroll, D. Gerace, I. Cristiani, and L. C. Andreani, "Optimizing polarization-diversity couplers for Si-photonics: reaching the -1dB coupling efficiency threshold," *Opt. Express* **22**(12), 14769–14781 (2014).
40. D. Benedikovic, P. Cheben, J. H. Schmid, D.-X. Xu, B. Lamontagne, S. Wang, J. Lapointe, R. Halir, A. Ortega-Moñux, S. Janz, and M. Dado, "Subwavelength index engineered surface grating coupler with sub-decibel efficiency for 220-nm silicon-on-insulator waveguides," *Opt. Express* **23**(17), 22628–22635 (2015).

41. G. Roelkens, D. Van Thourhout, and R. Baets, "High efficiency Silicon-on-Insulator grating coupler based on a poly-Silicon overlay," *Opt. Express* **14**(24), 11622–11630 (2006).
42. H.-Y. Chen and K.-C. Yang, "Design of a high-efficiency grating coupler based on a silicon nitride overlay for silicon-on-insulator waveguides," *Appl. Opt.* **49**(33), 6455–6462 (2010).
43. D. Vermeulen, S. Selvaraja, P. Verheyen, G. Lepage, W. Bogaerts, P. Absil, D. Van Thourhout, and G. Roelkens, "High-efficiency fiber-to-chip grating couplers realized using an advanced CMOS-compatible silicon-on-insulator platform," *Opt. Express* **18**(17), 18278–18283 (2010).
44. S. Yang, Y. Zhang, T. Baehr-Jones, and M. Hochberg, "High efficiency germanium-assisted grating coupler," *Opt. Express* **22**(25), 30607–30612 (2014).
45. W. S. Sacher, J. C. Mikkelsen, Y. Huang, J. C. C. Mak, Z. Yong, X. Luo, Y. Li, P. Dumais, J. Jiang, D. Goodwill, E. Bernier, P. G.-Q. Lo, and J. K. S. Poon, "Monolithically Integrated Multilayer Silicon Nitride-on-Silicon Waveguide Platforms for 3-D Photonic Circuits and Devices," *Proc. IEEE* **106**(12), 2232–2245 (2018).
46. M. Dai, L. Ma, Y. Xu, M. Lu, X. Liu, and Y. Chen, "Highly efficient and perfectly vertical chip-to-fiber dual-layer grating coupler," *Opt. Express* **23**(2), 1691–1698 (2015).
47. M. T. Wade, F. Pavanello, R. Kumar, C. M. Gentry, A. Atabaki, R. Ram, V. Stojanovic, and M. A. Popovic, "75% efficient wide bandwidth grating couplers in a 45 nm microelectronics CMOS process," in *IEEE Optical Interconnects Conference (OI, 2015)*, paper TuB4.
48. J. Notaros, F. Pavanello, M. T. Wade, C. M. Gentry, A. Atabaki, L. Alloatti, R. J. Ram, and M. A. Popovic, "Ultra-Efficient CMOS Fiber-to-Chip Grating Couplers," in *Optical Fiber Communication Conference (OFC, 2016)*, paper M2I.5.
49. L. Su, R. Trivedi, N. V. Sapra, A. Y. Piggott, D. Vercruyse, and J. Vučković, "Fully-automated optimization of grating couplers," *Opt. Express* **26**(4), 4023–4034 (2018).
50. A. Michaels and E. Yablonovitch, "Inverse design of near unity efficiency perfectly vertical grating couplers," *Opt. Express* **26**(4), 4766–4779 (2018).
51. C. Alonso-Ramos, P. Cheben, A. Ortega-Moñux, J. H. Schmid, D.-X. Xu, and I. Molina-Fernández, "Fiber-chip grating coupler based on interleaved trenches with directionality exceeding 95," *Opt. Lett.* **39**(18), 5351–5354 (2014).
52. D. Benedikovic, C. Alonso-Ramos, P. Cheben, J. H. Schmid, S. Wang, D.-X. Xu, J. Lapointe, S. Janz, R. Halir, A. Ortega-Moñux, J. G. Wangüemert-Pérez, I. Molina-Fernández, J.-M. Fédéli, L. Vivien, and M. Dado, "High-directionality fiber-chip grating coupler with interleaved trenches and subwavelength index-matching structure," *Opt. Lett.* **40**(18), 4190–4193 (2015).
53. X. Chen, D. J. Thomson, L. Crudginton, A. Z. Khokhar, and G. T. Reed, "Dual-etch apodised grating couplers for efficient fibre-chip coupling near 1310 nm wavelength," *Opt. Express* **25**(15), 17864–17871 (2017).
54. D. Benedikovic, C. Alonso-Ramos, D. Pérez-Galacho, S. Guerber, V. Vakarin, G. Marcaud, X. Le Roux, E. Cassan, D. Marris-Morini, P. Cheben, F. Boeuf, C. Baudot, and L. Vivien, "L-shaped fiber-chip grating couplers with high directionality and low reflectivity fabricated with deep-UV lithography," *Opt. Lett.* **42**(17), 3439–3442 (2017).
55. T. Watanabe, M. Ayata, U. Koch, Y. Fedoryshyn, and J. Leuthold, "Perpendicular Grating Coupler Based on a Blazed Antiback-Reflection Structure," *IEEE J. Light. Technol.* **35**(21), 4663–4669 (2017).
56. Y. Chen, R. Halir, I. Molina-Fernández, P. Cheben, and J.-J. He, "High-efficiency apodized-imaging chip-fiber grating coupler for silicon nitride waveguides," *Opt. Lett.* **41**(21), 5059–5062 (2016).
57. Y. Chen, T. Domínguez Bucio, A. Z. Khokhar, M. Banakar, K. Grabska, F. Y. Gardes, R. Halir, I. Molina-Fernández, P. Cheben, and J.-J. He, "Experimental demonstration of an apodized-imaging chip-fiber grating coupler for Si_3N_4 waveguides," *Opt. Lett.* **42**(18), 3566–3569 (2017).
58. FDTD Lumerical Solutions [Online]. Available: <https://www.lumerical.com>
59. L. Zavargo-Peché, A. Ortega-Moñux, J. G. Wangüemert-Perez, and I. Molina-Fernandez, "Fourier based combined techniques to design novel sub-wavelength optical integrated devices," *Prog. Electromagnetics Res.* **123**, 447–465 (2012).
60. S. M. Rytov, "Electromagnetic properties of a finely stratified medium," *Sov. Phys.* **2**, 466–475 (1956).
61. D. Oser, D. Pérez-Galacho, C. Alonso-Ramos, X. Le Roux, S. Tanzilli, L. Vivien, L. Labonté, and É. Cassan, "Subwavelength engineering and asymmetry: two efficient tools for sub-nanometer-bandwidth silicon Bragg filters," *Opt. Lett.* **43**(14), 3208–3211 (2018).
62. R. Halir, L. Zavargo-Peché, D.-X. Xu, P. Cheben, R. Ma, J. H. Schmid, S. Janz, A. Densmore, A. Ortega-Moñux, I. Molina-Fernandez, M. Fournier, and J.-M. Fédéli, "Single etch grating couplers for mass fabrication with DUV lithography," *Opt. Quantum Electron.* **44**(12–13), 521–526 (2012).
63. M. Passoni, D. Gerace, L. Carroll, and L. C. Andreani, "Grating couplers in silicon-on-insulator: The role of photonic guided resonances on lineshape and bandwidth," *Appl. Phys. Lett.* **110**(4), 041107 (2017).